Tuijin Jishu/Journal of Propulsion Technology
ISSN: 1001-4055
Vol. 45 No. 1 (2024)

Microstructural, Mechanical And Corrosion Properties Of Nano-Structured Az91 Magnesium Alloy Composites Fabricated By Spark Plasma Sintering

P. Mansoor [a] **, Dr. S. M Dasharath** [b*],
School of Mechanical Engineering, Reva university,
Bangalore, Karnataka 560064, India

Abstract

The study meticulously investigates the synthesis and characterization of nanocrystalline (nc) AZ91 magnesium alloy, achieved through a combination of mechanical ball milling and spark plasma sintering (SPS) techniques. It provides a detailed examination of the microstructural, mechanical, and corrosion behavior properties of the synthesized alloy. Specifically, the impact of an 8-hour ball milling process on grain particle refinement and the development of nanometer-sized grains is thoroughly analyzed. The subsequent sintering process, conducted for the AZ91 alloy at temperatures ranging from 465°C to 565°C using spark plasma sintering, is carefully discussed. Throughout the SPS process, the study observes a uniform distribution of grains with well-defined particle boundaries, and the absence of pores, indicating improved material integrity. Notably, a significant enhancement in mechanical properties, including hardness, tensile strength, and corrosion resistance, is noted in the AZ91 magnesium alloy with increasing sintering temperature. For instance, hardness reaches up to 62 Hv, while the highest UCS recorded is 342 MPa at 425°C, with a strain fracture of about 28%. Corrosion tests reveal the lowest corrosion rate at an Ecorr value of -1.362 mV vs SCE, an icorr value of 14.27 $\mu A.cm^{-2}$, and an rcorr value of 0.35 $mm.y^{-1}$ during the highest temperatures. This comprehensive exploration highlights the intricate relationship between processing techniques and material properties, underscoring the potential of nanocrystalline AZ91 magnesium alloy for various engineering applications due to its superior mechanical and corrosion-resistant characteristics. It offers valuable insights for further advancements in material science and engineering.

Keywords: Nanocrystalline, optical, physical, mechanical properties; spark plasma sintering.

1. Introduction

Magnesium (Mg) and its alloys have garnered significant attention due to their numerous advantageous properties such as low weight, high specific strength, and a low density of 1.74 g/cm^3, making them pivotal in aerospace, electronics, automotive, and household sectors. Recently, Mg and its alloys have emerged as potential candidates for biodegradable implant materials, replacing Ti-based alloys, stainless steels, and aluminum (Al) alloys owing to their superior mechanical properties, including higher tensile strength compared to aluminum alloys [5]. Despite possessing notable characteristics such as an elastic modulus of 41-45 GPa, magnesium alloys face challenges like low ductility, strength degradation at high temperatures, and inadequate corrosion resistance. Nanostructured metals, with grain sizes reduced to the nanometric scale, exhibit promising mechanical properties, as evidenced by previous research. Nanocrystalline materials, characterized by ultra-fine grain structures, demonstrate enhanced chemical and physical properties, including increased strength under compression, super plasticity at lower temperatures, and an inverse Hall-Petch relation for small nanometer grain sizes [3]. The synthesis of ultra-fine-grained Magnesium (Mg) alloy powders, achieved through Mechanical ball milling utilizing the SPEX 8000 shaker mill, yields grain sizes ranging from 1 to 100 nm. Severe Plastic Deformation (SPD) technologies such as ARB, HPT, SPS, and ECAP contribute to the consolidation of magnesium alloys, with research indicating successful microstructural modifications and enhanced mechanical properties under varying sintering temperatures. Spark Plasma Sintering (SPS) as shown in fig 1, a rapid sintering method, emerges as a viable technique for producing dense magnesium alloys with improved mechanical, biological, and

corrosion-resistant characteristics. The present research endeavors to explore the impact of Mechanical Ball milling on nanometer-sized grain production and investigates the microstructural, mechanical, and corrosion properties of dense nanocrystalline sintered specimens prepared through Spark Plasma Sintering (SPS) processes. Utilizing advanced characterization techniques like OM, XRD, SEM, and TEM, alongside ASTM standard testing methods, the study aims to comprehensively evaluate the performance of nanocrystalline AZ91 alloy samples, offering insights into their potential applications and future development pathways.

[1] explores the microstructure and mechanical properties of magnesium composites fabricated through Spark Plasma Sintering (SPS) technology. They elucidate the influence of processing parameters on the final properties of the composites, providing valuable insights into the optimization of SPS for enhancing the mechanical performance of magnesium alloys.

In their investigation, delve into the impact of nano-SiC reinforcement on the microstructure and mechanical properties of AZ91 magnesium alloy processed via Thixo molding. Their findings shed light on the potential of nanostructures to augment the mechanical strength and structural integrity of magnesium composites, offering new avenues for enhancing material performance in engineering applications.

[2] the relationship between β-phase morphology and corrosion behavior in the Mg alloy AZ91. Through their study, they reveal critical insights into the factors governing corrosion resistance in magnesium alloys, emphasizing the importance of microstructural features in mitigating environmental degradation and enhancing material durability. [3] delve into the initial stages of corrosion in AZ91D magnesium alloy immersed in a NaCl solution. Their research provides valuable insights into the early corrosion mechanisms, highlighting the alloy's susceptibility to environmental degradation and the imperative for developing effective corrosion mitigation strategies. [4] investigate the effects of Ca and Y additions on the microstructure and corrosion resistance of vacuum die-cast AZ91 alloy. Their study offers crucial insights into alloy modification strategies aimed at improving the corrosion resistance and overall performance of magnesium alloys in corrosive environments, thus advancing their applicability in diverse engineering applications. [5] delve into the mechanical milling of magnesium powder, elucidating the effects of milling parameters on the powder morphology and mechanical properties. Their research contributes to the understanding of powder processing techniques for enhancing the mechanical performance and formability of magnesium alloys, crucial for various manufacturing processes and applications. [6] investigate the microstructure and corrosion behavior of AZ91-0.4%Nd magnesium alloy. Their study provides valuable insights into the influence of Nd addition on the alloy's microstructural evolution and corrosion resistance, offering important considerations for alloy design and optimization in corrosion-sensitive applications. [7] examine the microstructure and mechanical properties of AZ91 magnesium alloy with minor additions of Sm, Si, and Ca elements. Their research elucidates the effects of alloying elements on microstructural refinement and mechanical enhancement, offering valuable insights for tailoring the properties of magnesium alloys to meet specific application requirements.

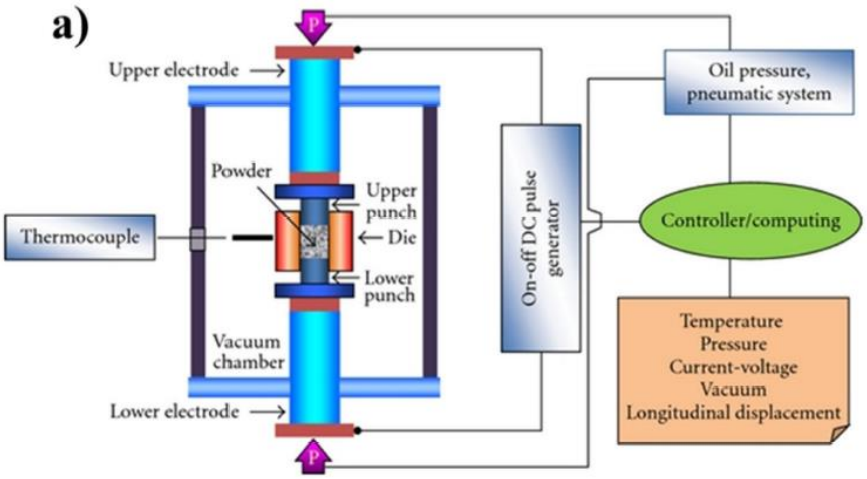

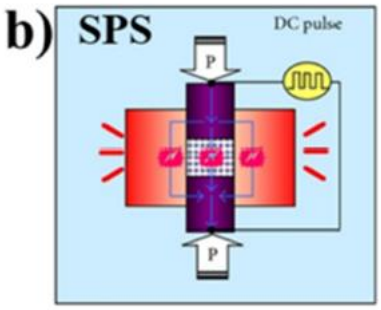

Figure 1. Schematic representation of (**a**) Spark plasma sintering; (**b**) SPS

2.Experimental Procedures

2.1 Materials and Sintering procedure

Commercially sourced magnesium (Mg) powder, with a purity of 99.6% and a particle size of 40µm (400 mesh), serves as the foundational material for creating the AZ91 alloy, featuring 3wt% Al, 1wt% Zn, 0.5wt% Mn, and 1.3wt% SiC as matrix components shown in table 1. Initially, the Mg AZ91 alloy undergoes an 8-hour mechanical ball milling process using the SPEX 8000 Shaker in an Argon atmosphere. The SPEX 8000 Shaker, a high-energy ball mill, operates between 0.2 to 10 grams of powders, utilizing a ball-to-powder ratio of 10:1 with 12.7mm diameter balls to minimize powder adhesion. The milled powder is then analyzed using a Siemens D5000 X-Ray diffractometer to determine particle size. Further characterization includes SEM and TEM analysis for grain size and fracture morphology, optical microscopy using the VHX-7000 Series Digital microscope, hardness testing with a HUAYIN HVS-1000A Vickers hardness tester, and relative density measurement via the Archimedes method [8-9]. Tensile tests are conducted following ASTM E8m standards, while corrosion resistance is evaluated using an electrochemical potentiodynamic workstation (EC-LAB BIOLOGIC SP-150) in a 0.1M NaCl solution at room temperature. Sintering temperatures, determined from literature, guide the fabrication process, with samples sintered at temperatures ranging from 425°C to 565°C using the SPS machine under a pressure of 60MPa, heating rate of 250°C/min, and holding time of 5 minutes. Below 425°C, sintering results in high porosity, as indicated by previous studies [10-13]. This comprehensive approach ensures thorough examination and optimization of the AZ91 alloy's properties for various applications.

Table 1: Chemical composition for AZ91 magnesium alloy

Elements	**Al**	**Zn**	**Mn**	**Si**	**Fe**	**Cu**	**Ni**	**Mg**
Contents /Wt. %	8.3-9.7	0.35-1.0	0.15-0.5	0.1	0.005	0.03	0.002	Bal.

2.2 Microstructure Characterization

The determination of the sintered sample's bulk density was conducted utilizing Archimedes' principle with an electronic balancer, boasting an accuracy of ±0.000g. Optical microscopy was employed to unveil the morphology of grain size, while a Scanning Electron Microscope (SEM) was utilized to scrutinize the distribution of particles within the sintered composite matrix materials [14-16]. To prepare the surface of the samples for examination, emery-based papers with a grit of 1500 were employed for grinding, followed by polishing with diamond paste less than 1µm in size. An acetic picrial/glycol solution was applied to reveal the grain boundaries of the sintered samples, enhancing the clarity and resolution of the observed features. These meticulous techniques contribute to a comprehensive understanding of the microstructure and characteristics of the sintered samples, aiding in the evaluation and optimization of their properties for various applications.

2.3 Mechanical Tests

The mechanical properties of the sintered samples were evaluated through hardness testing conducted using a Vickers hardness testing machine, applying an indenting load of 25g with a holding time of 15s. Tensile strength testing was performed according to ASTM standards. Specimens with a gauge part thickness of 3mm, width of 2mm, and length of 3mm were extracted from the sintered samples using an EDM machine. [17-19] The tensile tests were conducted using an Instron 5565 universal screw machine with a 5 KN capacity, operating at a crosshead speed of 0.5mm/min. The fractured surfaces resulting from the tensile tests were examined using a Scanning Electron Microscope (SEM), providing insights into the nature and characteristics of the fracture, thus contributing to a comprehensive understanding of the mechanical behavior of the sintered samples at table 2.

Table 2: Results of mechanical properties of sintered AZ91 at different temperatures

Alloy/ Temperatures	Density (g/cm^3)	Hardness (Hv)	Compressive strength (Mpa)
AZ91 at 465°C	99.89	62	342
AZ91 at 525°C	100.01	51.5	255.4
AZ91 at 565°C	100.23	42	246.7

3. Results and Discussion

3.1. Microstructure

The microstructural observations conducted on the Spark Plasma Sintered (SPSed) AZ91 alloy, spanning a sintering temperature range from 465°C to 565°C, reveal intriguing insights. Figures 2 and 3 illustrate the microstructural evolution during this temperature range. Optical microscopy reveals a uniform distribution of grains and particulates, particularly notable at higher temperatures, such as 565°C. SEM observations highlight well-defined bonds between grains, characterized by an equal amount of grain boundaries, indicative of a homogenized microstructure [20]. The phase distribution analysis, conducted via X-ray diffraction using a Siemens D5000 X-Ray diffractometer at a scan rate of 2°/min, as depicted in Figure 1, provides further elucidation. M. Mondet et al. [28], in their examination of SPSed AZ91 samples within a temperature range of 310°C to 500°C, observed the consistent appearance of precipitate $Al_{12}Mg_{17}$ along the grain boundaries across all temperature states [21-23]. These findings underscore the complex interplay between temperature, microstructure, and phase distribution, offering valuable insights into the mechanisms governing the sintering process and the resultant material properties of AZ91 alloy.

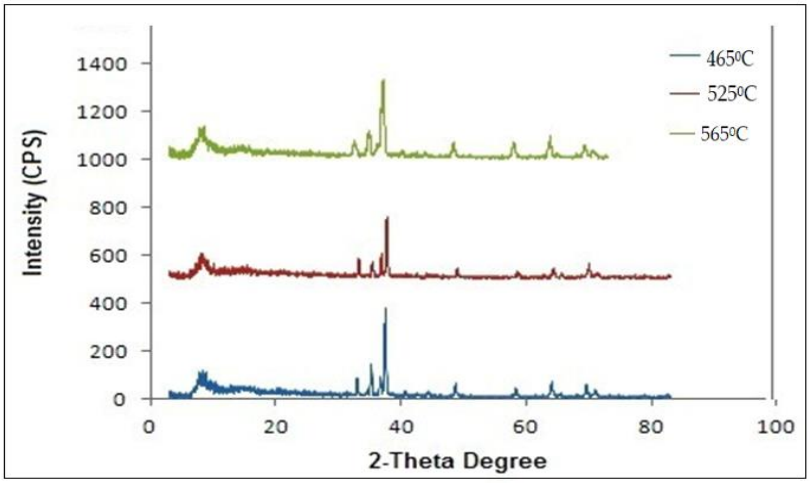

Fig.2.XRD Patterns for AZ91 at a)465^{0}C b)525^{0}C c)565^{0}C

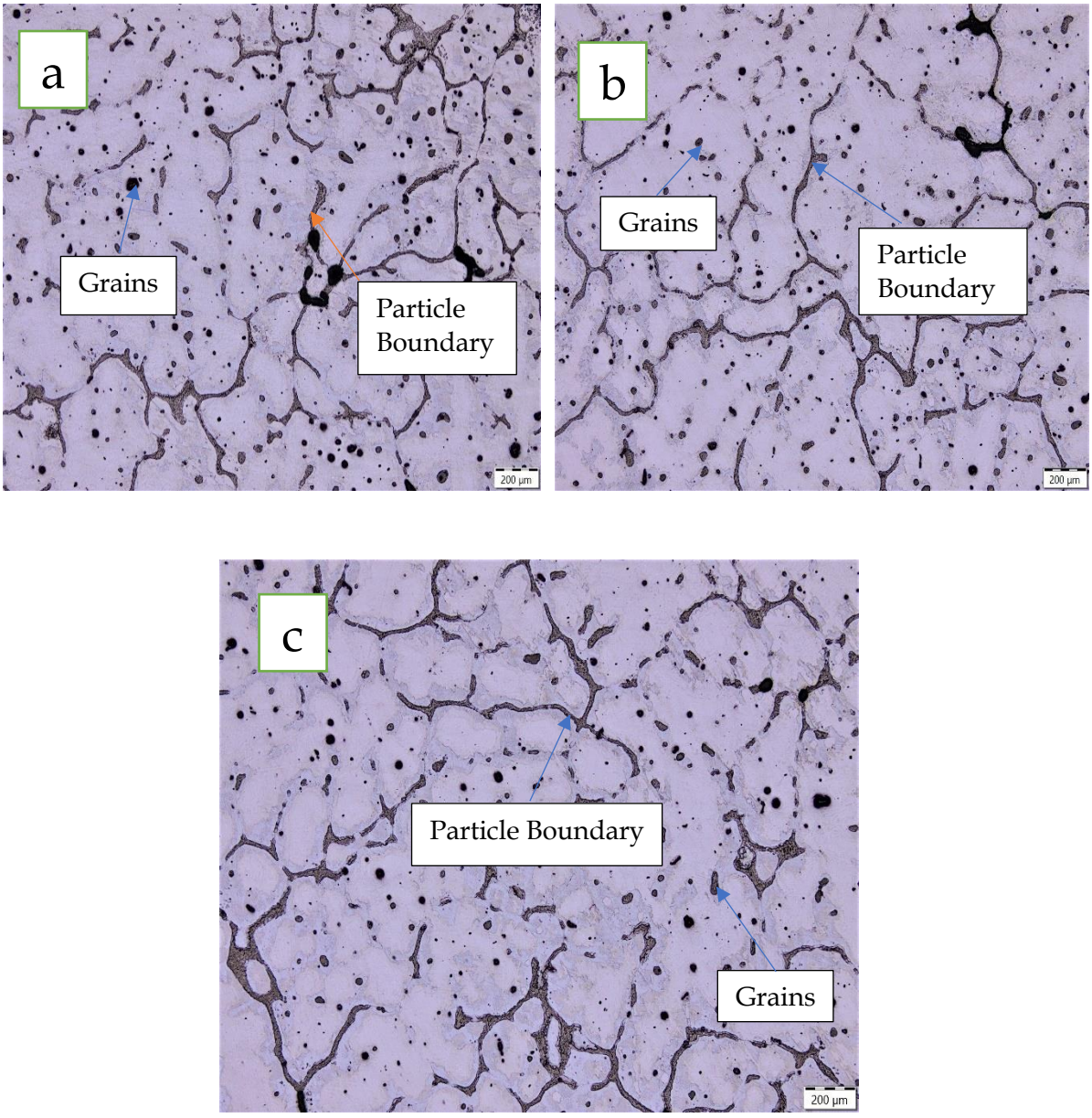

Fig.3. Optical Microstructure of AZ91 a)465^{0}C b)525^{0}C c)565^{0}C

3.1.2. Relative density

The density measurements of the Spark Plasma Sintered (SPSed) alloy AZ91 were conducted utilizing Archimedes' principle, boasting an accuracy range of ±0.000g. Intriguingly, the AZ91 alloy exhibited consistent density values across the sintered temperature range from 465°C to 565°C, as illustrated in Figure 4. M. Mondet et al. [26] observed a maximum density of 100 MPa for SPSed AZ91 samples within a temperature range of 310°C to 500°C. These findings suggest a robust and stable densification behavior of the AZ91 alloy across varied sintering temperatures, offering valuable insights into its mechanical properties and suitability for diverse applications.

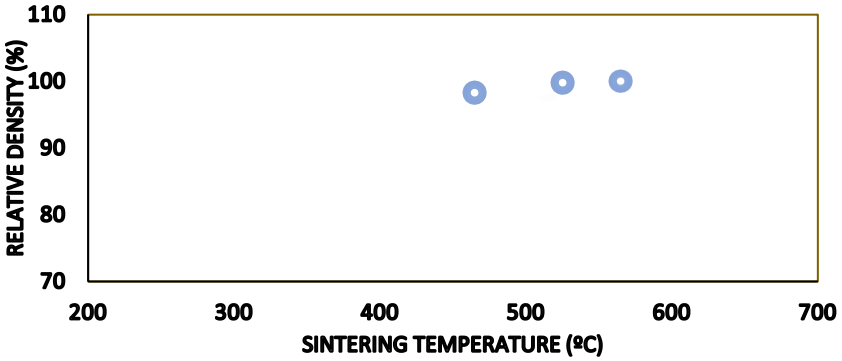

Fig 4. Relative Density of the AZ91 alloy samples sintered at a) 465^{0}C b) 525^{0}C c) 565^{0}C

3.1.3. Hardness

The hardness tests conducted on the Spark Plasma Sintered (SPSed) alloy AZ91 have revealed promising improvements, with hardness reaching 42Hv to 62Hv as sintering temperatures were elevated. This enhancement in hardness is attributed to the increased densification and density achieved during the sintering process, as illustrated in Figure 5. M. Mondet et al. [28] observed a similar trend, noting a hardness increase from 70 to 90 HV for SPSed AZ91 samples as sintering temperatures rose from 310°C to 500°C. These findings underscore the direct correlation between sintering conditions, material densification, and resulting mechanical properties, highlighting the potential for optimizing hardness through controlled sintering processes in AZ91 alloy fabrication.

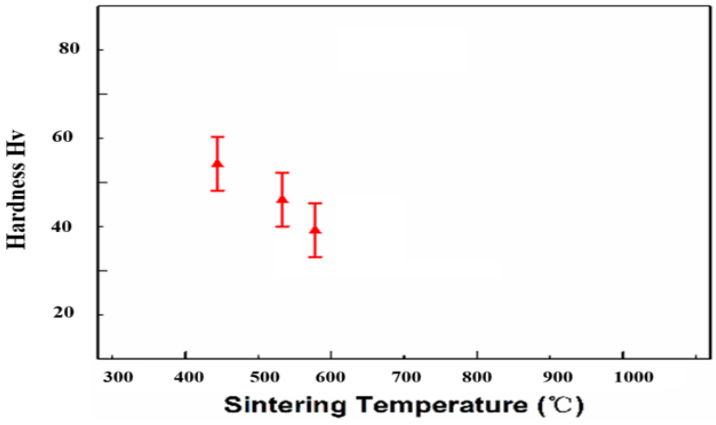

Fig 5. Hardness of the AZ61 alloy samples sintered at a) 465^{0}C b) 525^{0}C c) 565^{0}C

3.1.4. Compressive strength

The Uniaxial Compressive Strength (UCS) tests conducted on the Spark Plasma Sintered (SPSed) AZ91 alloy utilized the UTM Shimadzu TCE-N300A, with the test results plotted using engineering stress-strain, as depicted in Figure 6. The highest UCS achieved for the sintered specimen was approximately 342 MPa at 425°C, with a strain fracture of about 28%. This notable increase in UCS can be attributed to the higher densification of specimens achieved at elevated sintering temperatures. M. Mondet et al. [28] observed UCS test results for AZ91 during SPS, noting that at a temperature of 380°C, the highest UCS and strain for UCS were approximately 327 MPa and 13.7%, respectively. These findings underscore the influence of sintering temperature on the mechanical properties of the AZ91 alloy, highlighting the potential for achieving superior strength and ductility through optimized sintering conditions.

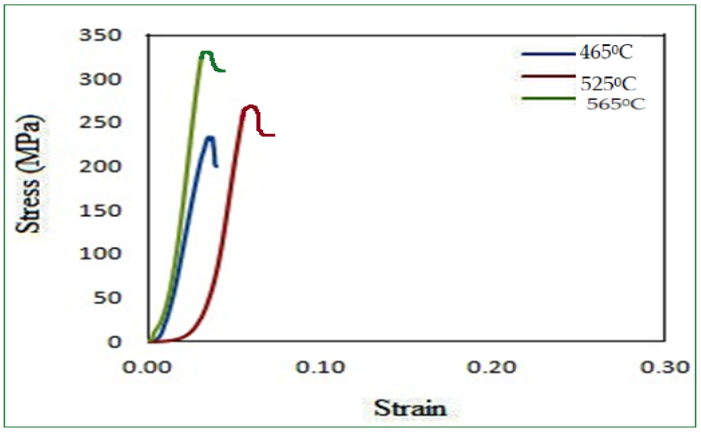

Fig 6. Compressive strength of the AZ91 alloy samples sintered at a) 465^0C b) 525^0C c) 565^0C

3.1.5. Fractography

The fractography analysis of AZ91, sintered within the temperature range of 465°C to 565°C, was conducted using SEM (Tesc an-Vega 3), as depicted in Figure 7. Observations reveal that at lower sintering temperatures, the fractures exhibit tearing edges and dimples. However, as the sintering temperatures increase, the tearing edges become less pronounced, indicating a reduction in ductile behavior. Instead, there is a noticeable increase in densification of the material [27]. This shift in fracture morphology suggests a transition in the material's mechanical response as a result of the sintering process, highlighting the importance of temperature control in tailoring the properties of AZ91 alloy for specific applications.

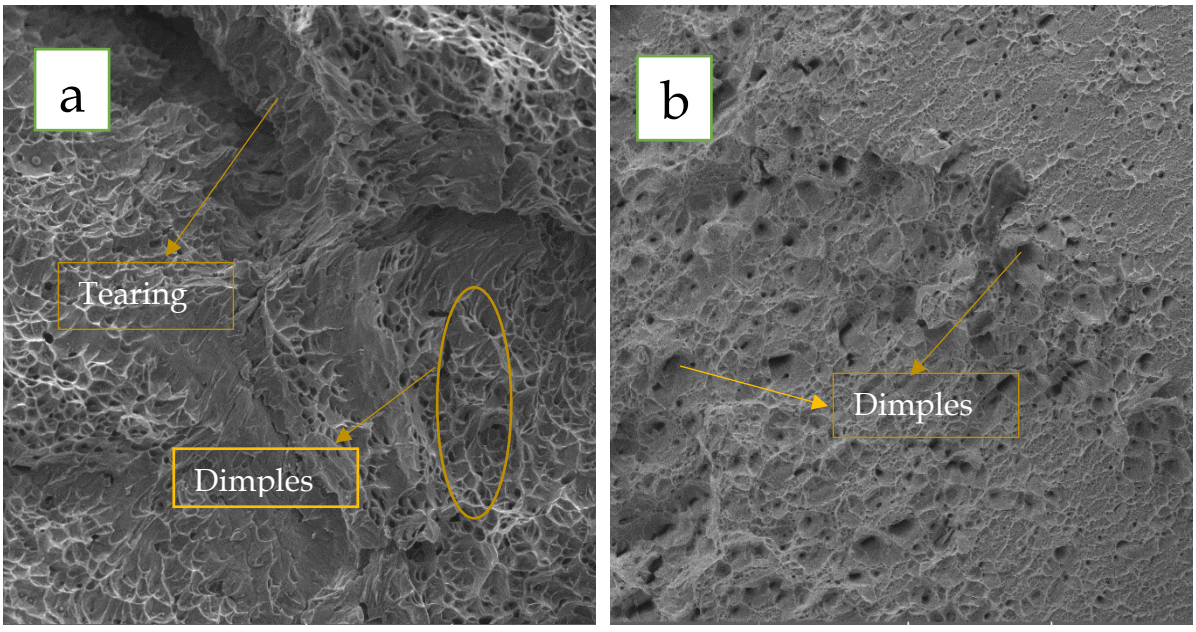

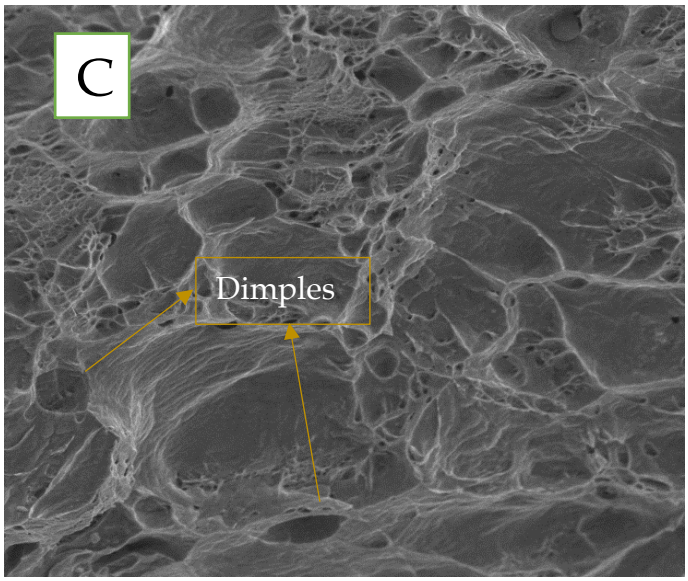

Fig 7. Facture morphology of the AZ91 alloy samples sintered at a) 465^{0}C b) 525^{0}C c) 565^{0}C

3.1.6. Potentiodynamic Polarization

The corrosion tests were conducted using the potentiodynamic polarization model type EC-LAB BIOLOGIC SP-150 for the SPS alloyed AZ61. The Potentiodynamic Polarization (PDP) tests were carried out over a duration of 7 hours, with the specimens exposed to a 0.1M NaCl solution at room temperature [24-25]. A three-electrode system was employed for PDP, with the reference electrode acting as a calomel electrode, the platinum electrode serving as the counter electrode, and the specimen exposed to the NaCl solution acting as the working electrode. The applied voltage ranged from -200 to +500 mV vs SCE (Saturated Calomel Electrode) with respect to the open circuit potential, and the scan rate was maintained at 1 mV.s^{-1}. Tafel fits provided by the EC-Lab software were utilized for curve analyses. Examination of the results revealed the lowest corrosion rate at an Ecorr value of -0.85 mV, an icorr value of 1.00E-04 µA.cm^{-2}, during the highest temperatures. Table 1 presents the test results for Electrochemical Polarization under the Electrochemical Polarization test Results section.

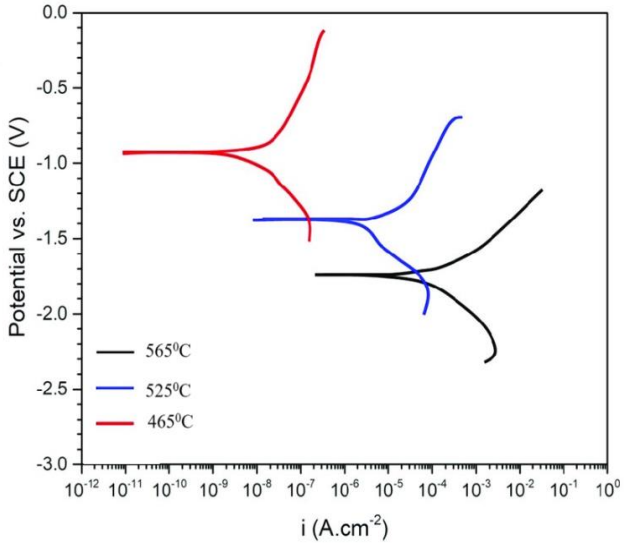

Figure 8. Potentiodynamic cures of (a) AZ91 alloy sintered at a) 465^{0}C b) 525^{0}C c) 565^{0}C

Table 3. Test outcomes for electrochemical polarization

Materials	Sintering Temperature (°C)	Ecorr (V vs SCE)	Icorr (A/cm^{-2})
AZ91	425	-1.05	1.00E-06
AZ91	525	-0.95	1.00E-05
AZ91	575	-0.85	1.00E-04

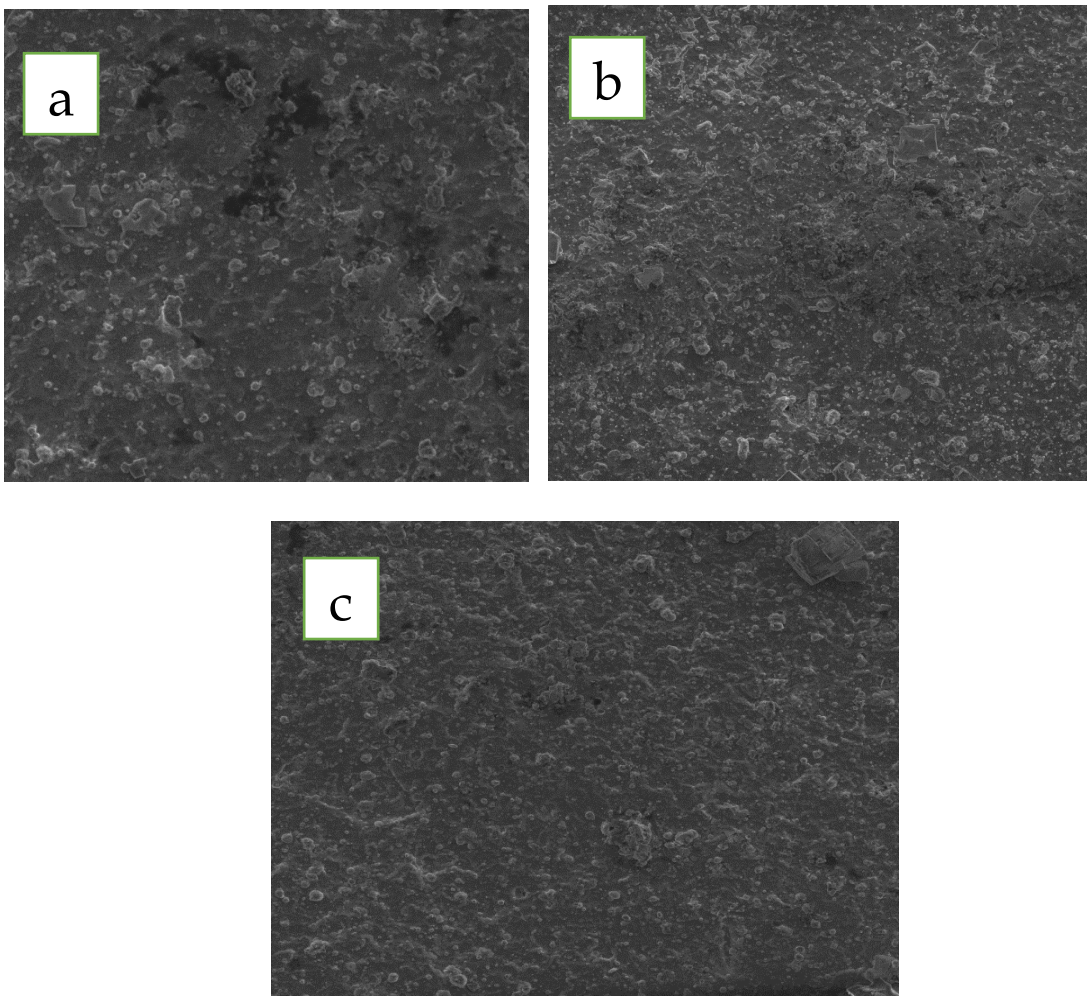

Fig 9. Corrosion images of the AZ91 alloy samples sintered at a) 465^0C b) 525^0C c) 565^0C

3.1.7. Wear Resistance

A pin on the disc (DUCOM Model: Wear & Friction Monitor TR-20) was used to conduct wear tests on the specimens. With a track diameter of 60mm, the pin was forced against a rotating disc. The sliding distance covered during the wear testing was approximately 3000 meters, with loads of 20 N and a speed of 2 m/s with spinning time of 2.5min/sec. The pined samples were 15 mm in diameter and 5 mm long. To ensure efficient contact with the steel disc, the pinned samples were treated with emery paper of an 80-grit size. Before and following each test, the samples are cleaned with acetone and weighed precisely to 0.0001 g. From the wear volume loss per unit sliding, the impact of the wear test was estimated. Using Fig. 10. As the sintering temperature rises, the wear rate improves while the wear rate declines.

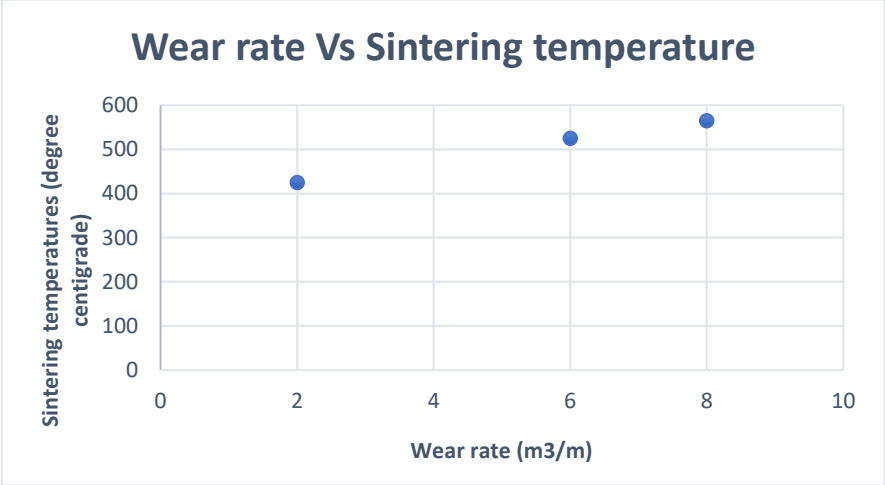

Figure 10. Wear Resistance of (a) AZ91 alloy samples sintered at a) 425^{0}C b) 525^{0}C c) 565^{0}C

The graph reveals a concerning trend, as the wear rate seems to climb steadily with increasing sintering temperature. At 425°C, the material exhibits a wear rate of approximately 2%, which doubles to 4% when pushed to 525°C. This rate further escalates to a worrying 6% at the extreme temperature of 565°C. This linear increase suggests a strong correlation between temperature and wear, highlighting the potential risks associated with operating the material at higher temperatures.

The SEM images i.e Fig 11. will give you the surface morphology of the alloy at different sintering temperatures [20-21]. Post wear test images of the specimen have revealed the presence of indistinct grooves and scratches are formed on the worn surface at lower temperatures. And the surface morphology got improved as the sintering temperature increased, there has been less worn surface as the temperature increased.

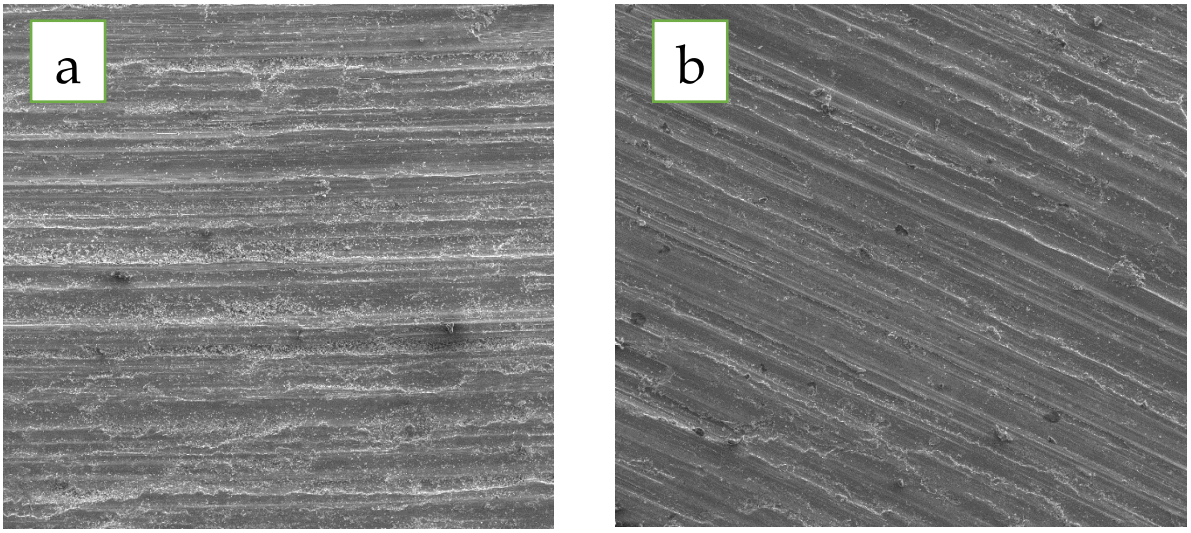

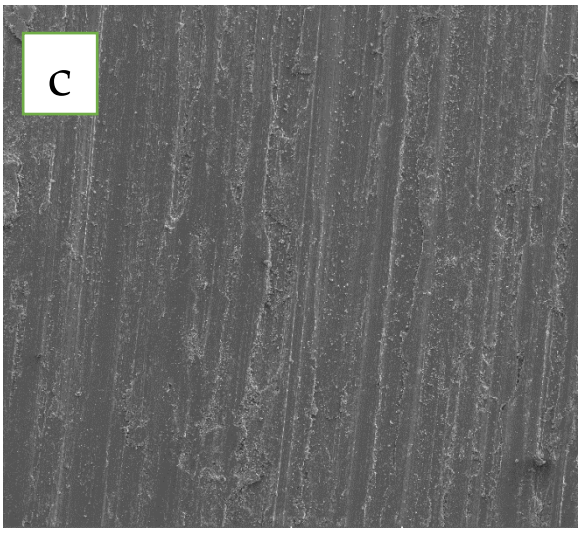

Fig 11. Wear Resistance of the AZ91 alloy samples sintered at a) 465^0C b) 525^0C c) 565^0C

4. Conclusion

The sintering process, carried out within the temperature range of 465°C to 565°C, demonstrated consistent densification across all temperatures, as evidenced by the Archimedes principle with an accuracy range of ±0.000g. Microstructural assessments revealed a uniform distribution of grains and particulates, with increased densification contributing to enhanced hardness, reaching up to 732 MPa with increasing sintering temperatures. Similarly, the Uniaxial Compressive Strength (UCS) tests conducted using the UTM Shimadzu TCE-N300A demonstrated an increase in strength, with the highest UCS recorded at 346 MPa at 565°C, along with a notable strain fracture of about 28%. Fractography analysis using SEM revealed a transition in fracture morphology from tearing edges and dimples at lower temperatures to reduced ductility and increased densification at higher temperatures. Corrosion tests conducted through potentiodynamic polarization indicated the lowest corrosion rate at an Ecorr value of -1.362 mV vs SCE, an icorr value of 14.27 $\mu A.cm^{-2}$, and an rcorr value of 0.35 $mm.y^{-1}$ during the highest temperatures. Overall, the findings suggest that increasing sintering temperatures in the AZ91 alloy fabrication process lead to improved densification, hardness, and corrosion resistance, while affecting fracture behavior, thus highlighting the importance of temperature control for optimizing the mechanical and corrosion properties of SPSed AZ91 alloy.

Acknowledgment

Authors wish to thank specific IIT Madras, India. for the Spark Plasma Sintering (SPS) process support of this research.

References

[1] Wan Nur Azrina Wan Muhammad, Yoshiharu Mutoh, Microstructure and mechanical properties of magnesium composites prepared by spark plasma sintering technology Journal of Alloys and Compounds 509 (2011) 6021–6029.
[2] S.Hwang, Nishimura, Mechanical milling of magnesium powder. Materials Science and Engineering A318 (2001) 22–33.
[3] Ming-Chun Zhao, Ming Liu,Influence of the β-phase morphology on the corrosion of the Mg alloy AZ91Corrosion Science 50 (7), 1939-1953.
[4] Vanessa Mandarano Pinela,1 Leandro Antônio de Oliveira,Study of the Corrosion Process of AZ91D Magnesium Alloy during the First Hours of Immersion in 3.5 wt.% NaCl Solution. Volume 2018, Article ID 8785154.

[5] H. Cui, G. Min, Effects of Be on microstructure, mechanical properties and corrosion resistance of AZ91 magnesium alloy.
[6] Ju Mei Zhang, Zhi Hu Wang,Microstructure and Corrosion Behavior of AZ91-0.4%Nd Magnesium Alloy. Applied Mechanics and Materials 291-294:2577-2580 · February 2013.
[7] Redeemina Comfort Bonnah, Yu Fu,Hai Hao,Microstructure and mechanical properties of AZ91 magnesium alloy with minor additions of Sm, Si and Ca elements. 16, pages319–325(2019).
[8] Xiao-yang Chen, Yang Zhang,Microstructure and mechanical properties of AZ91-Ca magnesium alloy cast by different processes. pages263–269(2018.
[9] HongminJia, XiaohuiFeng,Influence of solution treatment on microstructure, mechanical and corrosion properties of Mg-4Zn alloy. Volume 3, Issue 3, September 2015, Pages 247-252.
[10] YanHuang,DebaoLiu,Fabrication and characterization of a biodegradable Mg–2Zn–0.5Ca/1β-TCP composite. Volume 54, 1 September 2015, Pages 120-132.
[11] Claudio L. P. Silva Renata B. Soares,The Effect of High-Pressure Torsion on Microstructure, Hardness and Corrosion Behavior for Pure Magnesium and Different Magnesium Alloys. March 2019,1801081.
[12] Faraz Baradarani,Amir Mostafapou, Enhanced corrosion behavior and mechanical properties of AZ91 magnesium alloy developed by ultrasonic-assisted friction stir processing. January 2020, Pages 109-117.
[13] Feng Wang, Jibao Li, The Influence of Ca and Y on the Microstructure and Corrosion Resistance of Vacuum Die Casting AZ91 Alloy.
[14] Syam Prasad U, Kondaiah V, Akhil K, Effect of heat treatment on microstructure, microhardness and corrosion resistance of ZE41 Mg alloy. aki, výzkumné článk.
[15] Tingting Yang, Yuxin Ni, Microstructure, Mechanical Properties, In Vitro Degradation and Cytotoxicity of Mg-4Zn-3HA Alloy for Biodegradable Implant Materials. Journal of Hard Tissue Biology 23[1] (2014) 111-118.
[16] Aneta Kania, Ryszard Nowosielski, Mechanical and Corrosion Properties of Mg-Based Alloys with Gd Addition. Materials (Basel). 2019 Jun; 12(11): 1775.
[17] Andrzej Kiełbus,Tomasz Rzychoń, Microstructure and Mechanical Properties of Magnesium Alloys an d Composites. (ISSN 2073-4352).
[18] L. Hou1, Z. Li, Y. Pan,Microstructure, mechanical properties, corrosion behavior and hemolysis of as extruded biodegradable Mg-Sn-Zn alloy. AIP Conference Proceedings 1727, 020010 (2016).
[19] L. F. Guleryuz1, R. Ipek, I. Arıtman, Microstructure and mechanical properties of Zn-Mg alloys as implant materials manufactured by powder metallurgy method. AIP Conference Proceedings 1809, 020020 (2017).
[20] Dhyah Annur1, Franciska P. L.1, Aprilia Erryani,The synthesis and characterization of Mg-Zn-Ca alloy by powder metallurgy process AIP Conference Proceedings 1725, 020032 (2016).
[21] BioNanoMaterials | Volume 17: Issue 3-4, Investigating the effect of salicylate salt in enhancing the corrosion resistance of AZ91 magnesium alloy for biomedical application.
[22] Qiang Zhu, Ahmed Rassili, Stephen P. Midson and Xiao Gang Hu, Effect of Nano-SiC on Microstructure and Mechanical Properties of AZ91 Magnesium Alloy Processed by Thixo molding. Solid State Phenomena (Volume 285).
[23] Yunfei Ding, Cuie Wen,Effects of alloying elements on the corrosion behavior and biocompatibility of biodegradable magnesium alloys: a review. Royal society of chemistry, Issue 14, 2014.
[24] Wei-li Cheng, Yan-hui Liu, Microstructural Characteristics, Mechanical and Corrosion Properties of an Extruded Low-Alloyed Mg-Bi-Al-Zn Alloy. Mater., 20 March 2020 | https://doi.org/10.3389/fmats.2020.00055.
[25] Ya Zhang, Sen Wu1, Qiurong Chen,The Research on Corrosion Properties of Some Magnesium Alloys for Biomaterial. Int. J. Electrochem. Sci., 10 (2015) 1015 – 1026.
[26] Yuan Guangyin, Liu Manping, Ding Wenjiang, Mechanical Properties and Microstructure of Mg–Al–Zn–Si-base Alloy. Materials Transactions, Vol. 44, No. 4 (2003) pp. 458 to 462.
[27] Rajan Ambat, Naing Naing Aung, W. Zhou,Evaluation of microstructural effects on corrosion behavior of AZ91D magnesium alloy. Corrosion Science 42 (2000) 1433±1455.
[28] M. Mondet, E. Barraud Microstructure and mechanical properties of AZ91 magnesium alloy developed by Spark Plasma Sintering http://dx.doi.org/10.1016/j.actamat.2016.08.006.